Chemical reaction of protons with antiprotonic helium

Kazuhiro Sakimoto

Institute of Space and Astronautical Science, Japan Aerospace Exploration Agency, Yoshinodai 3-1-1, Chuo-ku, Sagamihara, Kanagawa 252-5210, Japan

(Received 6 March 2012; published 10 July 2012)

Collisions of protons p with antiprotonic helium atoms $\bar{p}\mathrm{He}^+$ (bound orbital states of an antiproton $\bar{p}$ and a helium ion He^+) are investigated from the viewpoint of chemical reaction. The $\bar{p}\mathrm{He}^+$ atoms with high orbital angular momentum quantum numbers $L > 40$ can be abundantly produced in the capture of $\bar{p}$ by metastable helium atoms $\mathrm{He}(2^{1,3}S)$. Since such orbital states are considered to be practically stable despite having Auger decay channels ($\bar{p}\mathrm{He}^+ \rightarrow \bar{p}\mathrm{He}^{2+} + e$), atomic and molecular collision processes involving $\bar{p}\mathrm{He}^+(L > 40)$ are experimentally measurable. In this study, adiabatic electron energies in the Born-Oppenheimer approximation are calculated for the $p + \bar{p}\mathrm{He}^+$ system. The $p + \bar{p}\mathrm{He}^+$ dynamical calculations of $\bar{p}$ exchange ($\rightarrow \bar{p}p + \mathrm{He}^+$) and dissociation ($\rightarrow p + \bar{p} + \mathrm{He}^+$) reactions on the ground-state adiabatic potential energy surface are carried out for various high orbital states of $\bar{p}\mathrm{He}$ by using a classical trajectory Monte Carlo method. The reaction cross sections and the state distributions of antiprotonic hydrogen atoms (protonium) $\bar{p}p$ produced in the exchange reaction are presented. If the orbital shape of $\bar{p}\mathrm{He}^+$ is near circular, the exchange reaction becomes inactive at low energies because the repulsive part of the interaction plays a critical role. In the $p + \bar{p}p$ system, however, the low-energy $\bar{p}$ exchange reaction remains active for any type of the initial $\bar{p}p$ orbital motion.

DOI: 10.1103/PhysRevA.86.012703 PACS number(s): 34.50.Lf, 34.20.Gj, 36.10.Gv

I. INTRODUCTION

In the study of molecular properties and molecular collision processes, a conventional and powerful tool is an adiabatic approach know as the Born-Oppenheimer (BO) approximation. The idea of this approximation is based on the fact that nuclei are much heavier than electrons. Antiprotons $\bar{p}$ also belong to the heavy particle group. However, the negative charge of $\bar{p}$ can be a disadvantage in applying the BO approximation to the system composed of atoms and antiprotons. For the antiprotonic system $\bar{p} + \mathrm{H}$, electronic bound states are missing at relative distances smaller than the so-called Fermi-Teller critical value ($R_{\mathrm{FT}} = 0.639$ a.u.) [1,2], and hence the BO approximation is not useful for the description of the collision processes even at very low energies. If the H atom is replaced with a He^+ ion (i.e., $\bar{p} + \mathrm{He}^+$), since there is no critical distance like R_{FT}, one may expect that the BO approximation is appropriate. However, the $\bar{p} + \mathrm{He}^+$ collisions were found to be very rich in prominent Feshbach resonances which are associated with electronic excited states and can also decay promptly into electronic continuum states $\rightarrow \bar{p}\mathrm{He}^{2+} + e$ [3]: this fact indicates that the BO approach is not a good approximation. The applicability of the BO approximation to the collision problem was suggested in the $\bar{p} + \mathrm{H}_2^+$ system [4]. Whether the target is an atomic or molecular ion is of fundamental difference. When the antiproton approaches one of the constituent protons of H_2^+, the electron can attach to the remaining proton. This is not the case for atomic ions: the electron has no such (adiabatic) escape route.

Recently, the present author investigated the $\bar{p} + \mathrm{H}_2^+$ collisions leading to the $\bar{p}$ exchange ($\rightarrow \bar{p}p + \mathrm{H}$) and dissociation ($\rightarrow \bar{p} + p + \mathrm{H}$) reactions [5]. The bound system $\bar{p}p$ is called antiprotonic hydrogen or protonium. The ground-state BO potential energy surface (PES) was calculated for various configurations in an *ab initio* manner, and the reaction processes on this PES were investigated in detail [5]. This procedure is exactly the same as established in a study of chemical reaction [6]. Later on, Cohen [7] applied a fermion molecular dynamics (FMD) method to the same system and obtained a good agreement with the BO approach. In the FMD method, the dynamical motion of the electron can be treated but classically (some quantum effects are assumed to be representable by the addition of pseudopotentials). The agreement between the BO and FMD methods suggests that the BO approximation is actually applicable to the $\bar{p} + \mathrm{H}_2^+$ system, although the classical treatment of the electron in the FMD method may be problematic. The BO approach has also been applied to collisions of negative muons μ^- with H_2^+ [8]. However, the agreement between the two methods is unsatisfactory for $\mu^- + \mathrm{H}_2^+$ [7]. One reason for this may be that the muon is only $\sim$200 times heavier than the electron. In a recent experimental study using a Penning trap apparatus by the ATHENA group [9], the evidence of the $\bar{p} + \mathrm{H}_2^+$ collisions leading to the $\bar{p}p$ formation was reported. It has become practically meaningful to verify that the process $\bar{p} + \mathrm{H}_2^+ \rightarrow \bar{p}p + \mathrm{H}$ can be classified as a chemical reaction in the sense mentioned above. In any case, the study of *antiproton chemistry* is quite primitive.

In the capture of $\bar{p}$ by He, high orbital states of antiprotonic helium atoms $\bar{p}\mathrm{He}^+$ are produced [10–12]. Actually, such states are embedded in electron continua and hence unstable due to an Auger process ($\bar{p}\mathrm{He}^+ \rightarrow \bar{p}\mathrm{He}^{2+} + e$). In this case, the $\bar{p}\mathrm{He}^+$ atom has a $1s$-state electron and should be distinguished from the resonance complexes in $\bar{p} + \mathrm{He}^+$ collisions. A few percent of the produced $\bar{p}\mathrm{He}^+$ have very long lifetimes and could be detected as (quasi) bound states in measurements [10–12]. It was found that the Auger transition is suppressed if $\bar{p}$ goes into a circular or near-circular orbit around He^+ [13–17]. This is considered to be the reason for the existence of the measurable long-lived $\bar{p}\mathrm{He}^+$ atoms. Furthermore, the molecular treatment in the BO approximation was found to be useful for the long-lived $\bar{p}\mathrm{He}^+$ [15–17]. (This is not the case for electronic excited states of $\bar{p}\mathrm{He}^+$ [3].) In

the $\bar{p}$ capture by metastable He($2^{1,3}S$), it is suggested that most of the produced $\bar{p}\mathrm{He}^+$ have orbital angular momentum quantum numbers $L > 40$ much higher than those produced in $\bar{p} + \mathrm{He}(1^1S)$ [18,19]. Since the Auger transition of $\bar{p}\mathrm{He}^+$ is strongly suppressed unexceptionally for any type of orbital motion if $L > 40$ [18,19], the $\bar{p}$ capture by metastable He is an efficient formation process of long-lived $\bar{p}\mathrm{He}^+$. Accordingly, one can expect that atomic and molecular collisions with $\bar{p}\mathrm{He}^+$ are also sufficiently measurable processes in experiments. Such interesting studies were made by Yamazaki and his collaborators [20–24]: the quenching cross sections of long-lived $\bar{p}\mathrm{He}^+$ in collisions with H_2 were measured. It is pointed out that the chemical reaction $H_2 + \bar{p}\mathrm{He}^+ \rightarrow H + \mathrm{He}^+\bar{p}H$ plays a decisive role in this quenching process. A further important finding is that the ground-state PES in the BO approximation is useful for understanding these experimental results [23–27].

As another realistic candidate of antiprotonic processes which can be regarded as a chemical reaction, the present paper considers $p + \bar{p}\mathrm{He}^+$ collisions. As in the case of $\bar{p} + H_2^+$, the two reaction channels $p + \bar{p}\mathrm{He}^+ \rightarrow \bar{p}p + \mathrm{He}^+$ ($\bar{p}$ exchange) and $\rightarrow p + \bar{p} + \mathrm{He}^+$ (dissociation) can take place on the ground-state PES obtained in the BO approximation, and no noticeable avoided crossing with excited electronic states exists on this PES. The $\bar{p}$ exchange reaction is also a way of producing $\bar{p}p$. In this study, the PES of the $p + \bar{p}\mathrm{He}^+$ system was calculated in an *ab initio* manner with satisfactory accuracy for the reaction calculations. Then, the exchange and dissociation reactions for various initial states of $\bar{p}\mathrm{He}^+$ were calculated by using a classical trajectory Monte Carlo (CTMC) method. The reaction cross sections and the state distributions of the products $\bar{p}p$ in the exchange reaction are reported. For comparison, the $\bar{p}$ exchange reaction in the $p + \bar{p}p$ system was also calculated.

II. POTENTIAL ENERGY SURFACE

In the BO approximation, the Hamiltonian of the $p + \bar{p}\mathrm{He}^+$ system is

$$H_{\mathrm{BO}} = -\frac{1}{2}\frac{\partial^2}{\partial \mathbf{s}^2} - \frac{2}{s} - \frac{1}{|\mathbf{s} - \mathbf{R}_p|} + \frac{1}{|\mathbf{s} - \mathbf{R}_{\bar{p}}|}, \qquad (1)$$

where $\mathbf{s}$ is the position vector of e from He^{2+} and $\mathbf{R}_p$ ($\mathbf{R}_{\bar{p}}$) is that of p ($\bar{p}$), as given in Fig. 1. Here and in the following, a.u. is used unless otherwise stated. The BO state can be defined by the following Schrödinger equation:

$$H_{\mathrm{BO}}\Psi(\mathbf{s}) = E_{\mathrm{BO}}(R_p, R_{\bar{p}}, \gamma)\Psi(\mathbf{s}), \qquad (2)$$

where the BO electron energy $E_{\mathrm{BO}}(R_p, R_{\bar{p}}, \gamma)$ is a function of R_p and $R_{\bar{p}}$ and the angle γ between $\mathbf{R}_p$ and $\mathbf{R}_{\bar{p}}$. In the limit of $R_p \rightarrow \infty$ and $R_{\bar{p}} \rightarrow \infty$, the BO energy $E_{\mathrm{BO}}(R_p, R_{\bar{p}}, \gamma)$ is equal to E_{He^+}, the ground-state energy of He^+. The PES of the $p + \bar{p}\mathrm{He}^+$ system can be written as

$$V(R_p, R_{\bar{p}}, \gamma) = E_{\mathrm{BO}}(R_p, R_{\bar{p}}, \gamma) + \frac{2}{R_p} - \frac{2}{R_{\bar{p}}} - \frac{1}{|\mathbf{R}_p - \mathbf{R}_{\bar{p}}|}. \qquad (3)$$

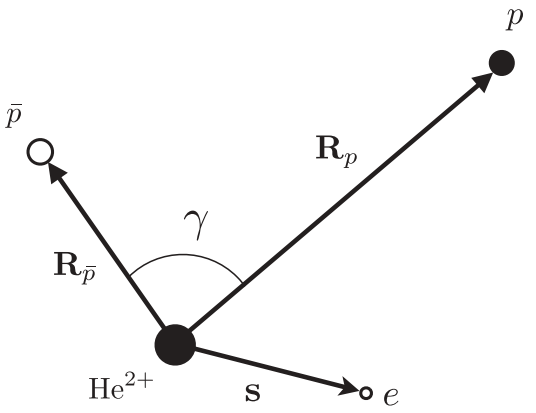

FIG. 1. Coordinates used in the calculation of the BO electronic state.

For large R_p, the PES is expressed in the following asymptotic form

$$V(R_p, R_{\bar{p}}, \gamma) = V(\infty, R_{\bar{p}}, \gamma) - \frac{D(R_{\bar{p}})\cos\gamma}{R_p^2}, \qquad (4)$$

where $D(R_{\bar{p}})$ is the dipole moment of $\bar{p}\mathrm{He}^+$. The BO potential can support bound channels only for $\bar{p}\mathrm{He}^+$ and $\bar{p}p$, but not for HeH^{2+} [28].

In the previous $\bar{p} + H_2^+$ study [4], the BO states were calculated by using spheroidal coordinates appropriate for two-center Coulomb nature of the homonuclear molecule H_2^+. In the present case, however the electron is always localized around He^{2+}, and hence one can employ a one-center treatment, in which the origin is located at He^{2+}. Equation (2) was solved by means of a grid-representation method [4], in which zero points of orthogonal polynomials were chosen as the grid points. The grid was constructed in polar coordinates with the z axis chosen along $\mathbf{R}_p$: 150 points of Laguerre polynomials for the radial distance s restricted to the range $s \leqslant 15$ a.u., 14 points of Legendre polynomials for the polar angle, and 5 points of Chebyshev polynomials for the azimuthal angle. The last choice corresponds to the inclusion of σ, π, and δ magnetic angular momenta of the electron. For the numerical check, the present BO energies of $\bar{p}\mathrm{He}^+$, $E_{\mathrm{BO}}(R_p = \infty, R_{\bar{p}}, \gamma)$, are compared in Table I with accurate values calculated by Shimamura [17]. For finite R_p, errors of the BO energies are expected to be in the same range.

Equation (2) was calculated at 49×49 points in the range $0 \leqslant R_p, R_{\bar{p}} \leqslant 10$ for each angle of $\gamma = 0°$, $30°$, $60°$, $90°$, $120°$, $150°$, and $180°$. As in Ref. [4], quadratic polynomial interpolation of E_{BO} was made with respect to $\log R_p$, $\log R_{\bar{p}}$, and γ. For $R_p > 10$ a.u., the PES was extrapolated from the value at $R_p = 10$ a.u. by using the R_p dependence of Eq. (4). For $R_p > 10$ a.u. and $R_{\bar{p}} > 10$ a.u., the extrapolation was made by using the asymptotic form

$$V(R_p, R_{\bar{p}}, \gamma) = E_{\mathrm{He}^+} + \frac{1}{R_p} - \frac{1}{R_{\bar{p}}} - \frac{1}{|\mathbf{R}_p - \mathbf{R}_{\bar{p}}|}. \qquad (5)$$

For the collinear ($\gamma = 0$) configuration of the $p + \bar{p}\mathrm{He}^+$ system, contour plots of the PES are shown in Fig. 2. An infinite wall (Coulomb repulsion) rises abruptly toward $R_p = 0$. The dissociation limit corresponds to the He^+ energy E_{He^+}.

TABLE I. BO electron energies (in a.u.) of $\bar{p}\mathrm{He}^+$.

$R_{\bar{p}}$ (a.u.)	Shimamura [17]	Present
0.0	−0.5000	−0.4997
0.1	−0.5123	−0.5110
0.2	−0.5466	−0.5451
0.5	−0.7435	−0.7413
1.0	−1.1174	−1.1132
1.2	−1.2306	−1.2260
1.4	−1.3226	−1.3177
1.6	−1.3973	−1.3923
2.0	−1.5094	−1.5042
4.0	−1.7506	−1.7453
6.0	−1.8334	−1.8282
8.0	−1.8750	−1.8698
10.0	−1.9000	−1.8947
∞	−2.0000	−1.9947

The two arrangement channels $p + \bar{p}\mathrm{He}^+$ and $\bar{p}\,p + \mathrm{He}^+$ are associated with the two infinitely deep valleys ($R_{\bar{p}} \simeq 0$ and $R_{\bar{p}} \simeq R_p$). The PES feature is somewhat similar to that in the ordinary molecular system except for these attractive Coulomb singularities.

Figure 3 shows the contour plots of the PES in Jacobi coordinates $(\mathbf{R},\mathbf{r})$ associated with the $p + \bar{p}\mathrm{He}^+$ arrangement. Here, the $\bar{p}\mathrm{He}^+$ atom is assumed to be a rigid rotor with $r = R_{\bar{p}} = 0.705$ a.u. In this case, $V \geqslant V(R_p = \infty)$ indicates the region of repulsive interaction in $p + \bar{p}\mathrm{He}^+$, and $V < V(R_p = \infty)$ indicates the attractive region. The PES reveals a quite asymmetric orientation dependence, namely, an infinitely high barrier (due to Coulomb repulsion) around He^+ and an infinitely deep well (due to Coulomb attraction) around $\bar{p}$. The PES is always strongly repulsive for $90^\circ \lesssim \theta \leqslant 180^\circ$ and is mostly attractive for $\theta \sim 0^\circ$. As the distance R decreases, the repulsive region prevails over the attractive region. It is evident

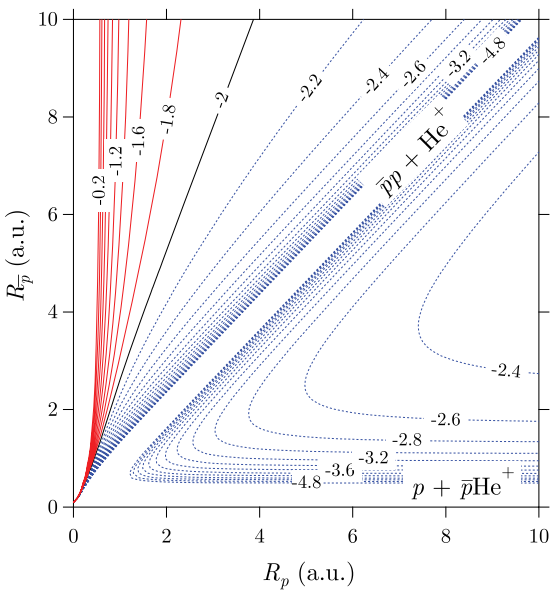

FIG. 2. (Color online) Contour plots of the potential energy surface (in a.u.) in the collinear ($\gamma = 0$) configuration. Solid lines: $V \geqslant E_{\mathrm{He}^+}$. Dotted lines: $V < E_{\mathrm{He}^+}$.

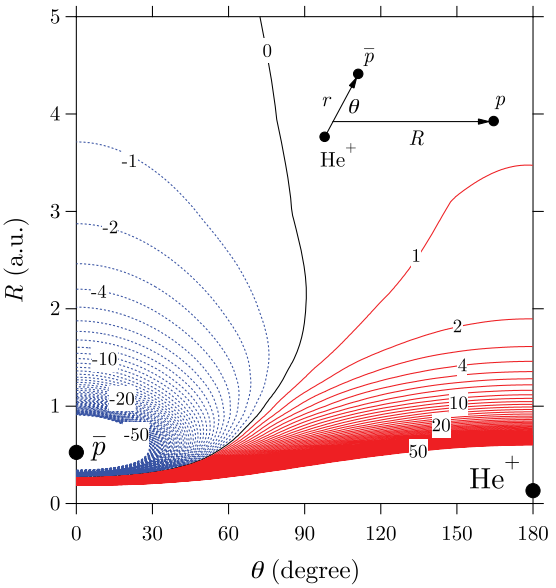

FIG. 3. (Color online) Contour plots of the potential energy surface (in eV) measured from $V(R_p = \infty)$ for the rigid rotor $\bar{p}\mathrm{He}^+$ with $r = R_{\bar{p}} = 0.705$ a.u.: $(\mathbf{R},\mathbf{r})$ are the Jacobi coordinates associated with the $p + \bar{p}\mathrm{He}^+$ arrangement, and θ is the angle between $\mathbf{R}$ and $\mathbf{r}$. Solid lines: $V \geqslant V(R_p = \infty)$. Dotted lines: $V < V(R_p = \infty)$.

that the collinear ($\theta \sim 0^\circ$) configuration is strongly preferred by the exchange reaction. The present system has a similarity to the ion and polar-molecule system. However, an essential difference from normal polar molecules is that the antiprotonic atom $\bar{p}\mathrm{He}^+$ is considered to be a pure dipole composed of completely separated opposite charges. The dipole nature still remains even at small R in the present system. (The $\bar{p}\,p$ atom is exactly a dipole.)

III. PROPERTIES OF ANTIPROTONIC ATOMS

For the $\bar{p}\,p$ atom, which is purely the hydrogenic system, the bound state is identified by the principal (n) and angular momentum (l) quantum numbers. For the $\bar{p}\mathrm{He}^+$ atom with an angular momentum quantum number L, the bound state can be recognized as the vibrational motion (with the quantum number $v = 0, 1, \ldots$) supported by the BO potential [17]. Since the Coulomb attraction plays a dominant role in the orbital motion, one may introduce the principal quantum number N defined by $N = v + L + 1$. Although the vibrational and rotational quantum numbers are limited to be finite for normal molecules, they can become infinite for $\bar{p}\mathrm{He}^+$. In Fig. 4, the orbital energies E_n of $\bar{p}\,p$ and E_{NL} of $\bar{p}\mathrm{He}^+$ are plotted as a function of the principal quantum number. The $\bar{p}\,p$ energies E_n are degenerate with respect to l ($\leqslant n - 1$). For the three-body system $\bar{p}\mathrm{He}^+$, such hydrogenic degeneracy is resolved. The $\bar{p}\mathrm{He}^+$ level structure is investigated in detail by Shimamura [17].

Although the interaction between $\bar{p}$ and He^+ is not a pure Coulomb form, the nature of the $\bar{p}\mathrm{He}^+$ orbital motion may be classified by the eccentricity $\kappa = [N^2 - L(L+1)]^{1/2}/N$, with $0 < \kappa \leqslant 1$ [29]. The motion having nonsmall κ is an extended elliptic orbit, and the one having $N = L + 1$ (i.e., $v = 0$) is usually called a circular state. Table II summarizes

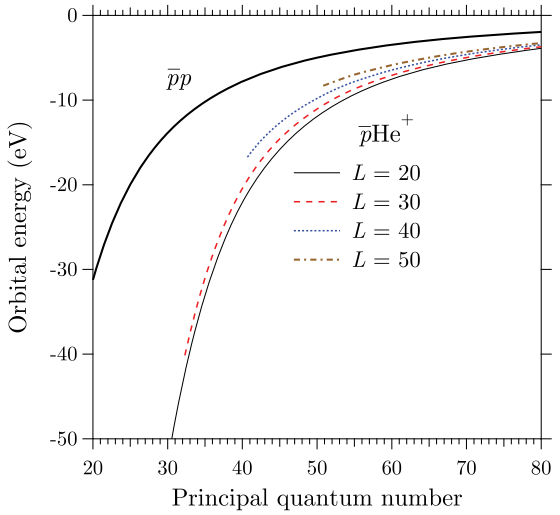

FIG. 4. (Color online) Orbital energies of $\bar{p}\mathrm{He}^+(N,L)$ and $\bar{p}p(n,l)$ measured from the dissociation limit $\bar{p}+p+\mathrm{He}^+(1s)$ as a function of the principal quantum number (N or n).

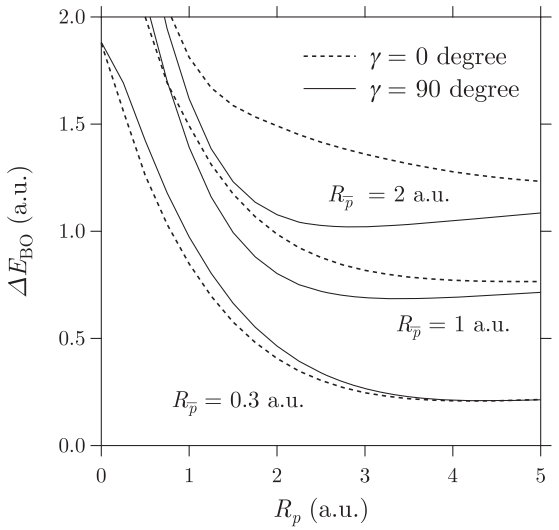

FIG. 5. Energy difference ΔE_{BO} between the ground and first-excited BO states in the $p+\bar{p}\mathrm{He}^+$ system ($\gamma = 0^\circ$ and 90° and $R_{\bar{p}} = 0.3$, 1.0, and 2.0 a.u.) as a function of the distance R_p.

the energy E_{NL}, the mean radius $\langle R_{\bar{p}}\rangle$, the inner turning point (perihelion) $R^-_{\bar{p}}$, the outer turning point (aphelion) $R^+_{\bar{p}}$, and the eccentricity κ for the states of $\bar{p}\mathrm{He}^+$ discussed in this study. The $\bar{p}\mathrm{He}^+$ atoms with the two lowest circular states in Table II have lifetimes against the Auger transition, $\tau = 1.6\,\mu$s for $(N,L) = (32,31)$ and $\tau = 2.7$ s for $(N,L) = (36,35)$ [14], which are long enough to justify the neglect of the Auger decay during collisions. The $\bar{p}\mathrm{He}^+$ atoms with $L \gtrsim 40$ and any N ($>L$) are practically stable [18,19]. The most vibrationally excited state shown in Table II is $(N,L) = (70,40)$ and has $v = 29$ and $\kappa = 0.816$. The quantum number n_c in Table II, given by setting $E_{n_c} = E_{NL}$, indicates the $\bar{p}p$ product state satisfying the condition of the energy matching in the exchange reaction. The rotational periods of the $\bar{p}\mathrm{He}^+$ circular states are, for example, ~40 a.u. for $(N,L) = (32,31)$ and ~1000 a.u. for $(N,L) = (61,60)$, which are much shorter than those of normal molecules. The $\bar{p}\mathrm{He}^+$ atoms are high-speed rotors as compared with the normal molecules.

TABLE II. Properties of $\bar{p}\mathrm{He}^+(N,L)$ obtained by using the present PES. Energies are in eV, and distances are in a.u.

(N,L)	E_{NL}	$\langle R_{\bar{p}}\rangle$	$R^-_{\bar{p}}$	$R^+_{\bar{p}}$	κ	n_c
(32,31)	−41.108	0.353	0.299	0.433	0.177	17
(36,35)	−26.865	0.475	0.401	0.573	0.167	22
(41,40)	−16.347	0.705	0.585	0.839	0.157	28
(45,40)	−12.685	1.045	0.477	1.401	0.436	31
(50,40)	−9.813	1.514	0.440	2.072	0.587	36
(51,50)	−8.247	1.525	1.291	1.765	0.140	39
(55,50)	−7.068	1.950	1.031	2.593	0.396	42
(61,40)	−6.264	2.694	0.410	3.701	0.748	45
(60,50)	−5.915	2.522	0.926	3.462	0.540	46
(61,50)	−5.718	2.643	0.913	3.636	0.561	47
(61,60)	−5.478	2.429	2.107	2.750	0.128	48
(65,60)	−4.814	2.904	1.724	3.808	0.366	51
(70,40)	−4.645	3.829	0.399	5.240	0.816	52
(70,50)	−4.314	3.814	0.837	5.275	0.693	54
(70,60)	−4.158	3.614	1.557	4.879	0.503	55

Figure 5 shows the energy difference ΔE_{BO} between the ground and first-excited BO states in the $p+\bar{p}\mathrm{He}^+$ system. If the difference ΔE_{BO} becomes small, one cannot neglect the nonadiabatic effect (i.e., electronic excitation) even at low collision energies. It is seen that the energy difference ΔE_{BO} increases mostly with decreasing R_p and is larger for larger $R_{\bar{p}}$. For a special case of $R_{\bar{p}} = 0$, the system is identical to H_2^+, and the $1s\sigma_g$ and $2p\sigma_u$ states become degenerate as $R_p \to \infty$. Therefore, the nonadiabatic effect may be important if the configurations with very small $R_{\bar{p}}$ contribute to the collisions. In the present case, however the $\bar{p}\mathrm{He}^+$ atoms are in very high L states, and hence the distance $R_{\bar{p}}$ cannot be small. From Table II, one can see $R_{\bar{p}} \gtrsim 0.3$ a.u., which means $\Delta E_{\mathrm{BO}} \gtrsim 0.2$ a.u. (Fig. 5). Thus, the direct electronic excitation would be negligible in the present system if the collision energy is much less than 1 keV.

Other than the Auger transition and direct electronic excitation, the present system has the following nonadiabatic reaction channel which is open even at low collision energies:

$$p + \bar{p}\mathrm{He}^+(N) \to \mathrm{H} + \bar{p}\mathrm{He}^{2+}(N_+), \tag{6}$$

where N_+ is the principal quantum number of $\bar{p}\mathrm{He}^{2+}$. This reaction is a charge transfer process. If N is very small (i.e., $\langle R_{\bar{p}}\rangle \ll 1$ a.u.), $\bar{p}\mathrm{He}^+$ is similar to the H atom. In this case, near-resonant charge transfer ($1s\sigma_g$ and $2p\sigma_u$ coupling) can take place. Since actually the energy matching in Eq. (6) can be achieved by $N_+ \simeq N$ only in the case of $N < 30$, the near-resonant charge transfer would be important for $N \ll 30$. If $N > 30$, the energy matching condition yields N_+ much lower than N (e.g., $N_+ \simeq 37$ for $N = 41$, $N_+ \simeq 40$ for $N = 51$, $N_+ \simeq 42$ for $N = 61$, and $N_+ = 44$ for $N = \infty$). The large difference $N - N_+$ suggests the inefficiency of the charge transfer process. Furthermore, the repulsion between p and $\bar{p}\mathrm{He}^+$ is significant for the He^+ side of $\bar{p}\mathrm{He}^+$ (cf., Fig. 3) unless $\langle R_{\bar{p}}\rangle$ is small, and the charge transfer $p + \mathrm{He}^+ \to \mathrm{H} + \mathrm{He}^{2+}$ has a very high threshold energy. As N increases, the charge

transfer process becomes negligible. In the present study, all the nonadiabatic processes are neglected.

IV. REACTION CALCULATION

The dynamical calculations were performed for the $p + \bar{p}\mathrm{He}^+$ collisions on the present adiabatic PES using the Jacobi coordinates $(\mathbf{R},\mathbf{r})$; and the exchange and dissociation reaction processes,

$$\begin{aligned} p + \bar{p}\mathrm{He}^+(N,L) &\rightarrow \bar{p}p(n,l) + \mathrm{He}^+, \\ p + \bar{p}\mathrm{He}^+(N,L) &\rightarrow p + \bar{p} + \mathrm{He}^+, \end{aligned} \tag{7}$$

were investigated for various initial states (N,L) of $\bar{p}\mathrm{He}^+$. Since highly excited states are involved in both the reactant and product channels, an accurate quantum mechanical treatment is quite difficult for these processes. Thus, the CTMC method was adopted in the present study. Because of the negative charge of $\bar{p}$, Eq. (7) bears similarities to charge transfer and ionization in ion collisions with Rydberg atoms. In the case of the Rydberg atom targets, the CTMC calculations have been carried out by several workers and compared with experimental results [30–32]. These studies indicate that the CTMC method is useful at least for the qualitative understanding of the collision processes. It should be mentioned that the heavy mass of $\bar{p}$ further encourages the use of the CTMC method for the present reaction processes.

Most of the details of the trajectory calculations are the same as described previously [5]. The vibrational and rotational action variables were restricted to have the correct quantized values at the start of the collision. The initial relative distance R between p and $\bar{p}\mathrm{He}^+$ was chosen as $>30R_{\bar{p}}^+$. The center-of-mass collision energy E was considered to be $E = 1 \sim 50$ eV. Other initial collision parameters were Monte Carlo selected as appropriate. For the initial $\bar{p}\mathrm{He}^+$ states discussed in this study, the exchange channels are always open at all the collision energies, and the dissociation channel is closed unless $E \geqslant |E_{NL}|$.

Figure 6 illustrates trajectory examples of excitation (nonreactive), dissociation, and exchange collisions for $(N,L) = (41,40)$ at $E = 50$ eV. For these three trajectories, the same values were chosen as the initial dynamical variables except that the initial vibrational action angles were only slightly different from each other. As a result, all the trajectories are very similar until just before the closest approach of p to $\bar{p}\mathrm{He}^+$. However, they become quite different finally after the collision. Such sensitive dependence of the initial conditions is due to the strong Coulomb attraction working between p and $\bar{p}$. These examples also indicate that the exchange and dissociation channels are in competition if the dissociation channel is open. Furthermore, an interesting thing is that the reaction can occur even when p is far from $\bar{p}\mathrm{He}^+$; namely, the interaction range of the reaction is larger than the mean radius $\langle R_{\bar{p}} \rangle$.

Figure 7 shows the dependence of the exchange and dissociation probabilities on the impact parameter b for $(N,L) = (41,40)$ at several collision energies. In the CTMC calculation corresponding to a fixed impact parameter, 1000 trajectories were run. It turns out that the contribution to the reaction cross section comes from the impact parameters up

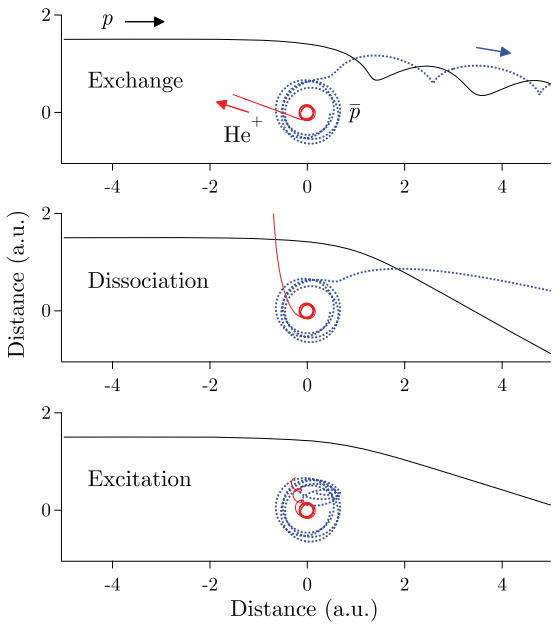

FIG. 6. (Color online) Trajectories, revealing excitation, dissociation, and exchange collisions, projected onto the plane of the initial $\bar{p}\mathrm{He}^+$ rotation in the Lab frame for $(N,L) = (41,40)$ and $E = 50$ eV. The initial collision plane is set to be identical to the rotation plane of $\bar{p}\mathrm{He}^+$. The impact parameter is 1.5 a.u. The $\bar{p}\mathrm{He}^+$ orbits are drawn from the start of the collision. The initial condition is the same for the three trajectories except that the initial vibrational action angle is larger by 0.02π for the dissociation trajectory and by 0.05π for the exchange trajectory than that for the excitation trajectory.

to $b_{\max} \simeq 2.5$ a.u., which is four times larger than the mean radius $\langle R_{\bar{p}} \rangle$ and three times larger than the outer turning point

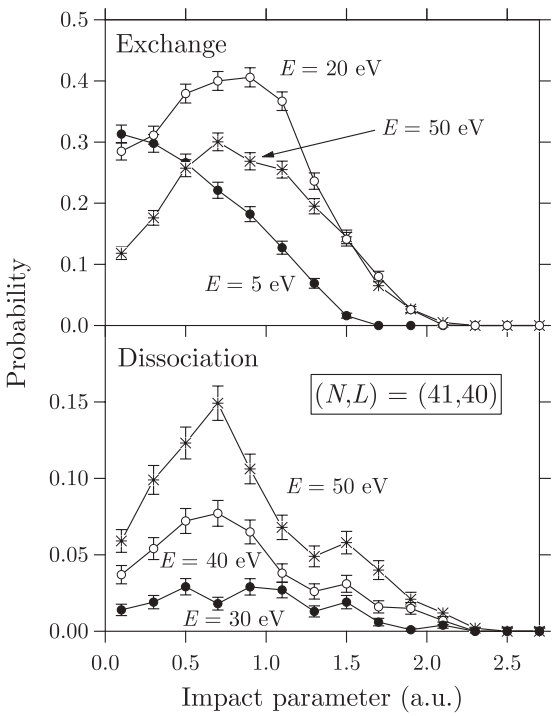

FIG. 7. Impact-parameter dependence of the reaction probabilities for $(N,L) = (41,40)$. The error bars are due to the statistical standard deviation.

$R_{\bar{p}}^{+}$. Unlike the case of $\bar{p} + H_2^+$ collisions [5], the sum of the exchange and dissociation probabilities is always less than 0.5. This reflects the fact that the Coulomb repulsion works between p and He^+ in the present system.

In the CTMC calculation of the exchange (σ_{ex}) and dissociation (σ_{dis}) cross sections, the impact parameter b was also randomly varied in the range $0 \leqslant b \leqslant b_{max} = 4\langle R_{\bar{p}} \rangle \sim 5\langle R_{\bar{p}} \rangle$, and 10 000 trajectories were run. By specifying the final state n or l of the products $\bar{p}p$ as was done previously [5], one can calculate the partial exchange cross sections $\sigma_{ex}(n)$ or $\sigma_{ex}(l)$. Then, the mean quantum numbers of $\bar{p}p$ produced in the exchange reaction may be defined by $\langle n \rangle = \sum_n n\sigma_{ex}(n)/\sigma_{ex}$ and $\langle l \rangle = \sum_l l\sigma_{ex}(l)/\sigma_{ex}$.

V. REACTION CROSS SECTIONS

First, the calculation of the exchange cross section σ_{ex} was carried out for the $\bar{p}He^+$ atoms in the circular states $(N,L) = (32,31),(36,35)$, and $(41,40)$ which were associated with the existing experimental studies [10–12]. The results are shown in Fig. 8(a) in the range of collision energies $E = 1$–50 eV. It is found that the exchange cross section

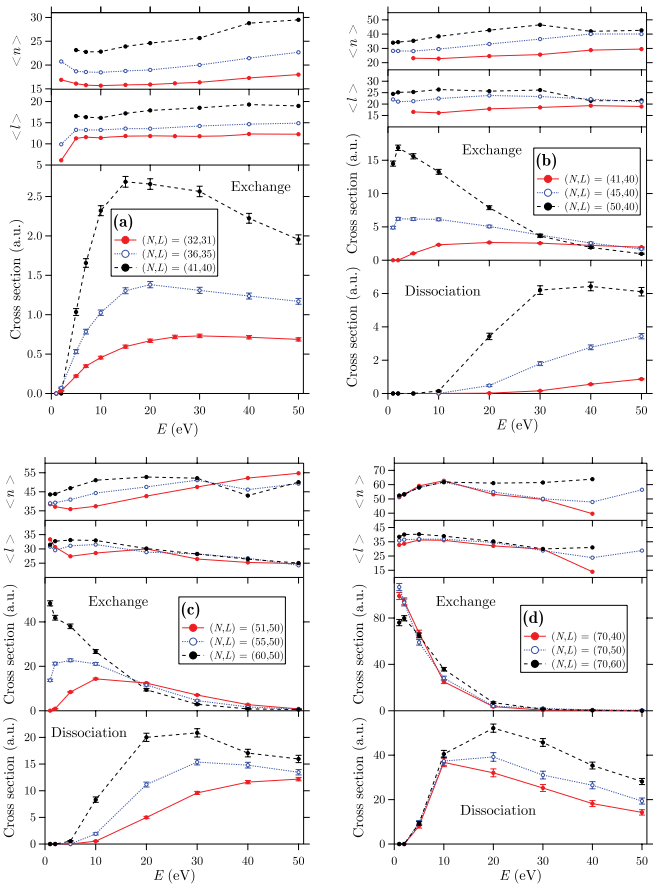

FIG. 8. (Color online) Reaction cross sections (σ_{ex} and σ_{dis}) and mean quantum numbers ($\langle n \rangle$ and $\langle l \rangle$) as a function of the collision energy E. The error bars are due to the statistical standard deviation. (a) The circular states: $(N,L) = (32,31)$, $(36,35)$, and $(41,40)$. (b) The $L = 40$ states: $(N,L) = (41,40)$, $(45,40)$, and $(50,40)$. (c) The $L = 50$ states: $(N,L) = (51,50)$, $(55,50)$, and $(60,50)$. (d) The $N = 70$ state: $(N,L) = (70,40)$, $(70,50)$, and $(70,60)$.

becomes very small and vanishes at low energies $E \lesssim 2$ eV, and it takes the maximum at an energy far above 10 eV. As expected, the cross section becomes larger with increasing N. Since the dissociation reaction is less significant at these energies, the dissociation cross section is not shown in this figure.

Figures 8(b) and 8(c) show the reaction cross sections for the same L (= 40 and 50) and different N. Since the dissociation reaction becomes important at $E \leqslant 50$ eV for $N \gtrsim 40$, the dissociation cross sections σ_{dis} are also plotted. The dissociation cross section increases with energies from the threshold $|E_{NL}|$ and becomes noticeable at energies higher than $E = E_0$ providing the local maximum peak of the exchange cross section. The dissociation is the dominant reaction channel at high energies $E \gg E_0$. It is understood also from these energy dependencies that a competitive relationship exists between the exchange and dissociation channels. For the same L, the exchange cross section is larger for higher N at low energies, but rather an opposite tendency is observed at high energies. The latter fact is considered to be due to the increased significance of the dissociation channel at the high energies.

The reaction cross sections for the same $N = 70$ and different L are plotted in Fig. 8(d). In contrast to Figs. 8(a)–8(c) showing the results for different N, the cross sections (except for the dissociation at $E > 10$ eV) are not largely different among the (70,40), (70,50), and (70,60) states. This is considered to be the same reason for the fact that the $\bar{p}He^+$ orbital energies E_{NL} and also the mean radius $\langle R_{\bar{p}} \rangle$ are strongly dependent on N but not so on L (cf., Fig. 4 and Table II). Thus, it is expected that also the reaction processes are characterized by E_{NL} or $\langle R_{\bar{p}} \rangle$.

Figure 9 shows the exchange and dissociation cross sections for all the states presented in Table II at a fixed collision energy ($E = 10$, 30, and 50 eV), plotted against E_{NL}. On the whole, the reaction cross sections for each E may be regarded as a smooth function of E_{NL}. Although the exchange cross section is decreasing at high E_{NL} for $E = 30$ and 50 eV, the total reaction cross section given by the sum $\sigma_{tot} = \sigma_{ex} + \sigma_{dis}$ seems to be a monotonically increasing function of E_{NL} for all the collision energies. Thus, one can conclude that a high orbital energy promotes the total combined reactivity of the exchange and dissociation channels.

It is naturally expected that the reaction cross section correlates closely with the geometrical size of $\bar{p}He^+$. For some states, the exchange cross section has a local maximum peak in the present energy range (Fig. 8). In Fig. 10, the largest data values of the exchange cross sections for such states are plotted against $\langle R_{\bar{p}} \rangle^2$. One can see that all these exchange cross sections are roughly proportional to $\langle R_{\bar{p}} \rangle^2$ and are approximated by $7.06\langle R_{\bar{p}} \rangle^2$. The fact that the maximum cross section is more than twice as large as the geometrical cross section $\pi\langle R_{\bar{p}} \rangle^2$ of $\bar{p}He^+$ indicates that the $\bar{p}$ exchange process in $p + \bar{p}He^+$ is a very active reaction.

VI. LOW-ENERGY BEHAVIOR

An interesting finding in Fig. 8 is that the exchange cross sections for the circular states become zero at low energies $E \lesssim 2$ eV despite the fact that a lot of product channels are

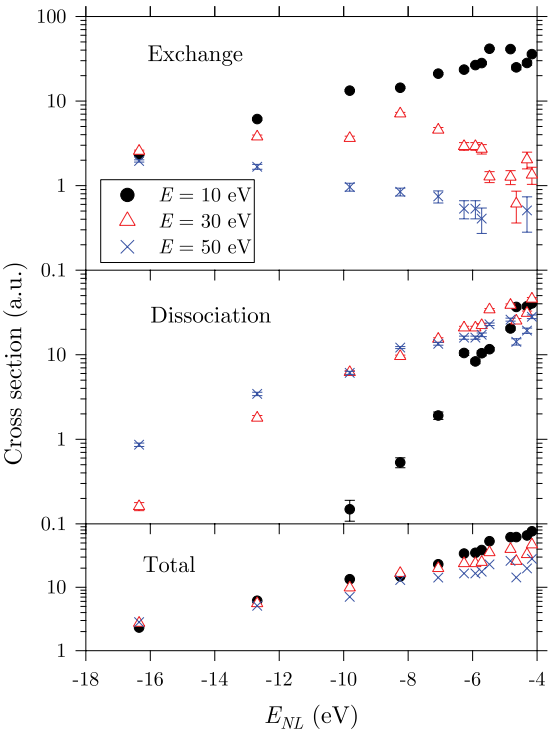

FIG. 9. (Color online) Reaction cross sections (σ_{ex}, σ_{dis}, and $\sigma_{tot} = \sigma_{ex} + \sigma_{dis}$) for all the states presented in Table II at $E = 10$, 30, and 50 eV as a function of the $\bar{p}He^+$ energy E_{NL}. The error bars are due to the statistical standard deviation.

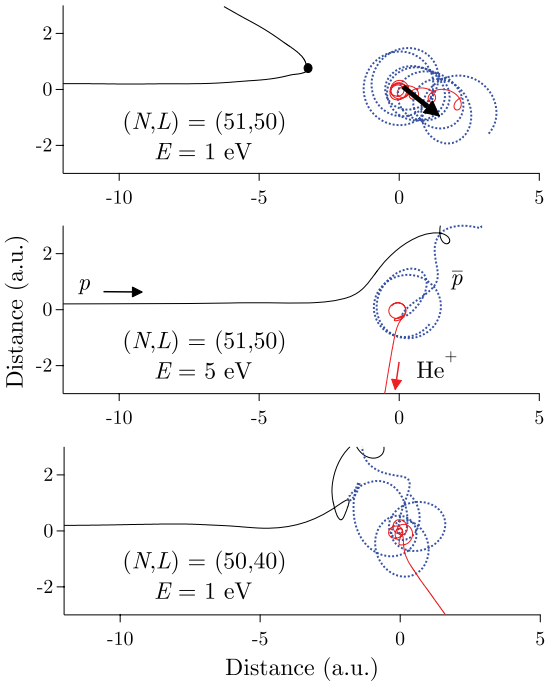

FIG. 11. (Color online) Illustrative examples of trajectories projected onto the plane of the initial $\bar{p}He^+$ rotation in the Lab frame for $(N,L) = (51,50)$ at $E = 1$ and 5 eV and for $(N,L) = (50,40)$ at $E = 1$ eV. The initial collision plane is set to be identical to the rotation plane of $\bar{p}He^+$. The impact parameter is 0.2 a.u. The trajectories are drawn from the time at which p just appears in the display area of the graph. In the top panel, the bold arrow indicates the vector $\mathbf{r}$ ($=\mathbf{R}_{\bar{p}}$) at the time when p reaches the closest (turning) point (indicated by the solid circle).

open even at $E = 0$. This suggests that the circular states are quite stable against collisions with surrounding low-energy ions. For the noncircular states $(N,L) = (60,50)$, (70,50),

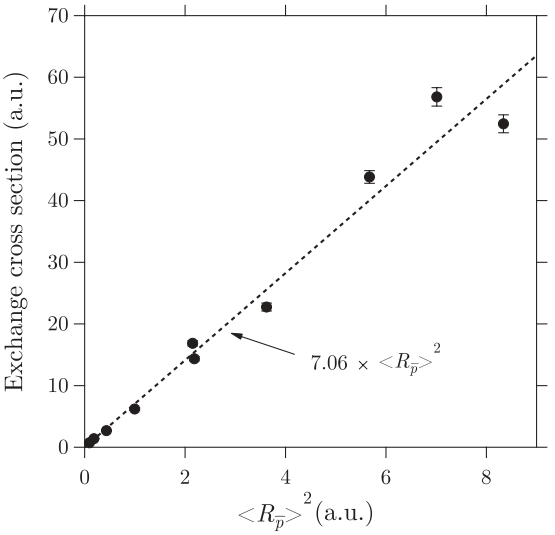

FIG. 10. The largest value of the exchange cross section σ_{ex} in the present calculation each for $(N,L) = (32,31)$, (36,35), (41,40), (45,40), (50,40), (51,50), (55,50), (61,40), (61,60), and (65,60), plotted against $\langle R_{\bar{p}} \rangle^2$. The error bars are due to the statistical standard deviation. The dotted line indicates the proportional relation with the constant 7.06 a.u., which is the mean value of $\sigma_{ex}/\langle R_{\bar{p}} \rangle^2$.

and (70,40) which have large eccentricities $\kappa > 0.5$, the exchange cross section increases with decreasing E. For the other noncircular states, the exchange cross section remains nonvanishing at $E = 1$ eV, but has a tendency to decrease with decreasing E at very low energies. For gaining a better understanding of the low-energy behavior of the cross section, Fig. 11 shows some illustrative examples of trajectories for the circular $(N,L) = (51,50)$ and noncircular (50,40) states. It can be seen for $(N,L) = (51,50)$ that the incident p is reflected at a relative distance R much larger than the size of $\bar{p}He^+$ at $E = 1$ eV. Furthermore, the He^+ side of $\bar{p}He^+$ points in the direction of p (i.e., $\theta \sim 180^\circ$) when p arrives at the reflection (turning) point. (The same feature is commonly observed also in other low-energy trajectories for the circular states.) This indicates that the repulsive part of the interaction can work effectively for the reflection of p and keeps p at a distance from $\bar{p}He^+$. If the collision energy is sufficiently high (the middle panel of Fig. 11), p can make a close approach to $\bar{p}He^+$, which results in the exchange reaction. For $(N,L) = (50,40)$, however the effect of the repulsion seems to be apparently less significant, and the exchange reaction can take place at low energies (the lowermost panel of Fig. 11).

In Fig. 3, the PES is shown for $R_{\bar{p}} = 0.705$ a.u., which corresponds to $\langle R_{\bar{p}} \rangle$ of $\bar{p}He^+$ in the circular state $(N,L) = (41,40)$. It is seen that, for example, the repulsive barrier with a height $\geqslant 1$ eV exists at $R \lesssim 3.5$ a.u. if $\theta \sim 180^\circ$ and

at $R \lesssim 1.5$ a.u. if $\theta \sim 90^\circ$. Therefore, if the collisions for $(N,L) = (41,40)$ and $E = 1$ eV occur in the perpendicular ($\theta \sim 90^\circ$) configuration, the incident p is always reflected by the repulsive barrier at $R \sim 1.5$ a.u., which is outside the main interaction region of the exchange reaction (Fig. 7). Next, let us assume that the collisions occur in the coplanar configuration. The time for the passage of p across the critical region $R \lesssim 3.5$ a.u. is ~ 500 a.u., while the rotational period of $\bar{p}\mathrm{He}^+$ with $(N,L) = (41,40)$ is ~ 120 a.u. Therefore, the He^+ side of $\bar{p}\mathrm{He}^+$ points in the direction of the incident p several times during the passage across the critical region, and p can be surely reflected by the repulsive part ($\theta \sim 180^\circ$) of the interaction before the close encounter. Thus, the repulsive part can play a decisive role in the low-energy collisions. This happens because the $\bar{p}\mathrm{He}^+$ atom is a high-speed rotor. If the rotation were slow as in the case of normal molecules, the situation might be quite different: The rotation would be easily hindered or become a libration with decreasing R, and the attractive part could play a more decisive role than the repulsive part. The interaction between p and $\bar{p}\mathrm{He}^+$ at $\theta = 180^\circ$ is roughy estimated by $R^{-1} - (R + \langle R_{\bar{p}} \rangle)^{-1}$. For $(N,L) = (51,50)$, this gives the barrier height >1 eV at $R \lesssim 5.5$ a.u., and the time for the passage across the critical region is $\sim$790 a.u., compared with the rotational period which is $\sim$420 a.u., which is roughly proportional to $\langle R_{\bar{p}} \rangle^{3/2}$ (the third of Kepler's laws [29]). Thus, increasing N decreases the rotation number during the passage across the critical region in which the barrier height is higher than a certain value, and hence the effect of the repulsion remains insignificant until the collision energy becomes lower.

If the difference $N - L$ (or the eccentricity κ) is large, the orbital motion of $\bar{p}\mathrm{He}^+$ forms a long ellipse though its major axis rotates, as seen in Fig. 11. If the aphelion side of the ellipse happens to be directed toward p, the effective strength of the repulsion would be considerably reduced as compared to the case of the circular orbit. (In the case of the opposite orientation, the significance of the repulsion would increase effectively.) For large $N - L$, thus some of the incident p can find an access route to $\bar{p}\mathrm{He}^+$, and the exchange cross section remains finite at very low energies. The type of the $\bar{p}\mathrm{He}^+$ motion, a circular or elliptic orbit, is an important factor having an influence on the low-energy exchange reaction. In the limit as $E \to 0$, if not all the incident p were reflected by the repulsive part of the interaction at large distances, the exchange cross section would diverge as $E^{-1/2}$, which is typical of the ion-molecule system. Probably, the exchange cross section for noncircular states having $\kappa \sim 1$ diverges at $E \to 0$.

For $\bar{p}\mathrm{He}^+$, the orbital energies of the same N states are not degenerate with respect to L. This is considered to play an important role in maintaining the $\bar{p}\mathrm{He}^+$ orbital shape during the collision. If the target is $\bar{p}p(n,l)$, then the angular momentum l is easily varied within the degeneracy ($l \leqslant n-1$) even at large $p + \bar{p}p$ separations (as exemplified by the presence of the linear Stark effect), and hence the orbital shape can be no longer maintained in the important interaction region. Therefore, one can expect that the selectivity behavior of the exchange reaction for the orbital type is missing for the $p + \bar{p}p$ collisions. In the present study, the CTMC calculation of the $\bar{p}$ exchange cross section was carried out also for

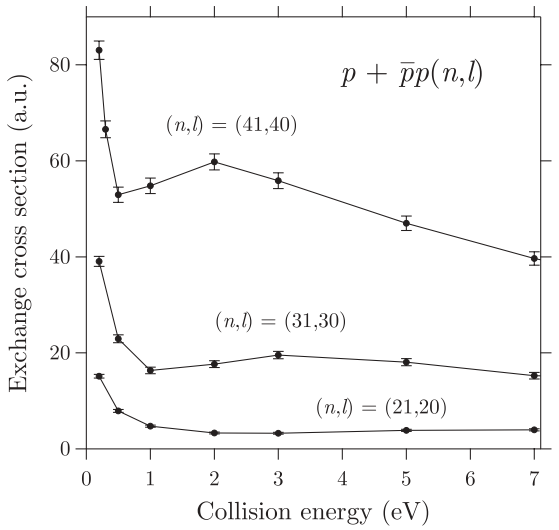

FIG. 12. Cross sections for the exchange reaction $p + \bar{p}p(n,l) \to \bar{p}p + p$ with $(n,l) = (21,20)$, (31,30), and (41,40) as a function of the collision energy. The error bars are due to the statistical standard deviation.

$p + \bar{p}p(n,l)$ initially in the circular states $(n,l) = (21,20)$, (31,30), and (41,40), and the results are shown in Fig. 12. The two protons were treated as distinguished particles. It can be actually seen that the cross section increases at very low energies. It should be remembered furthermore that the strong l mixing induced by external charged particles is also the cause for the increased instability of $\bar{p}p$ due to annihilation [33–35].

Yamazaki *et al.* [20–24] investigated the quenching processes of $\bar{p}\mathrm{He}^+$ by H_2 collisions at temperatures $T = 15$–300 K. They found that the quenching cross section rapidly decreases for $(N,L) = (37,34)$ and (38,37) and not so for $(N,L) = (39,35)$ at low temperatures. The low-temperature behavior for $(N,L) = (37,34)$ and (38,37) was explained in terms of an activation barrier and a quantum tunneling effect. Sauge and Valiron [25,26] calculated the ground-state PES in the BO approximation and showed the possibility of the existence of an activation barrier in $\mathrm{H}_2 + \bar{p}\mathrm{He}^+$ and also in $\mathrm{He} + \bar{p}\mathrm{He}^+$. However, the activation barrier is not directly clarified simply by viewing the PES, as also in the present case (cf., Fig. 3). To deduce the effective activation energy, Sauge and Valiron [25,26] averaged out the interaction over the orientation of $\bar{p}\mathrm{He}^+$ assuming its free rotation. This treatment can be justified because the collision time is much longer than the rotational period of $\bar{p}\mathrm{He}^+$. In the present case, such rotational averaging is meaningless since the collision time is at most only several times longer than the rotational period for $E \simeq 1$ eV and $L \gtrsim 30$. In addition, no activation barrier could be found at $R \gg \langle R_{\bar{p}} \rangle$ actually in the effective potential obtained by a simple orientation averaging for the circular states. In this study, no simplified model was able to be introduced for verifying the presence of the effective activation barrier. Probably, it is absolutely necessary to accurately take account of all the rotational, vibrational, and translational motions for understanding the $\bar{p} + \mathrm{He}^+$ collision dynamics at $E \sim 1$ eV.

VII. PRODUCT-STATE DISTRIBUTION

For investigating the state distribution of the products $\bar{p}p(n,l)$ in the exchange reaction, the partial cross sections $\sigma(n)$ and $\sigma(l)$ were calculated for various initial states (N,L). Figure 13(a) shows the distributions at the collision energy $E \simeq E_0$ for the three circular states $(N,L) = (41,40)$, $(51,50)$, and $(61,60)$. As N increases, the peak of the distribution moves toward higher n or l. The distributions for $(N,L) = (41,40)$ at other energies are shown in Fig. 13(b), and it can be seen that the position of the peak does not change so much with the collision energies. The n and l distributions for the same $L(=40)$ and different N are shown in Fig. 13(c). As in Fig. 13(a), the peak moves toward higher n or l with increasing N. The distributions for the same $N(=61)$ and different L are shown in Fig. 13(d). In this case, the peak positions and also the distribution shapes are not so much different from each other. As in the case of the total exchange cross section $\sigma_{\rm exc}$, the orbital energy E_{NL} is an important parameter characterizing also the product-state distributions.

For the circular states of $\bar{p}\mathrm{He}^+$, the peak position of the distribution $\sigma(n)$ is close to that of $\sigma(l)$. This is because near-circular states of $\bar{p}p$ are abundantly produced from the circular states of $\bar{p}\mathrm{He}^+$. As $N-L$ increases, however the difference between the peak positions of $\sigma(n)$ and $\sigma(l)$ becomes large. Thus, it turns out that the circular states of $\bar{p}p$ are most efficiently produced from the circular states of $\bar{p}\mathrm{He}^+$.

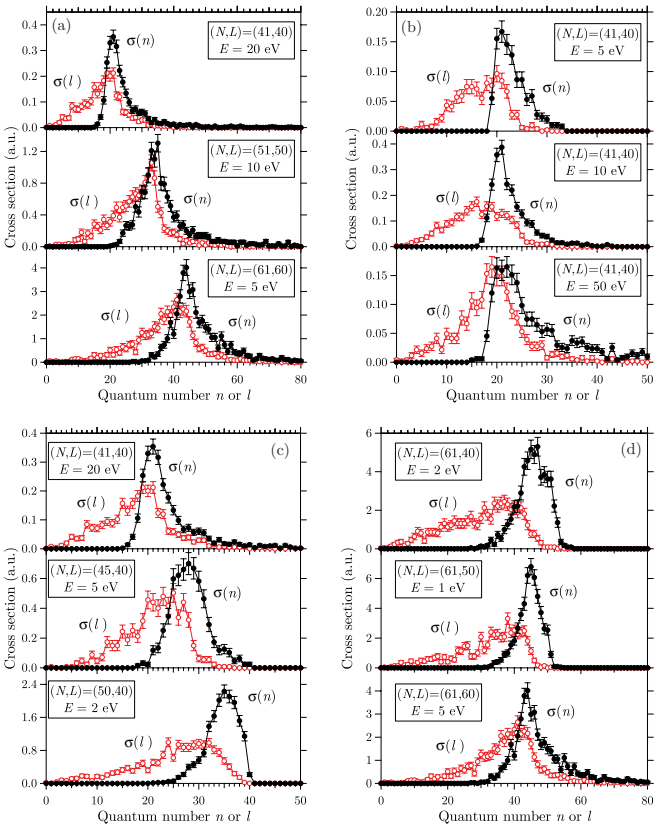

FIG. 13. (Color online) n and l distributions of $\bar{p}p$ [$\sigma_{\rm ex}(n)$ and $\sigma_{\rm ex}(l)$]. The error bars are due to the statistical standard deviation. (a) $(N,L) = (41,40)$, $(51,50)$, and $(61,60)$ and $E \simeq E_0$. (b) $(N,L) = (41,40)$ and $E = 5$, 10, and 50 eV. (c) $(N,L) = (41,40)$, $(45,40)$, and $(50,40)$ and $E \simeq E_0$. (d) $(N,L) = (61,40)$, $(61,50)$, and $(61,60)$ and $E \simeq E_0$.

The distributions can be classified into two types having a sharp cutoff tail [e.g., $E = 5$ eV in Fig. 13(b)] and a loosely decreasing tail [e.g., $E = 50$ eV in Fig. 13(b)]. This can be understood from energetics, which gives the allowed values of n as

$$n < \begin{cases} n_{\max} = \left[\frac{m_{\bar{p}p}}{2(|E_{NL}|-E)}\right]^{1/2} & \text{if} \quad E < |E_{NL}|, \\ \infty & \text{if} \quad E \geqslant |E_{NL}|, \end{cases} \tag{8}$$

where $m_{\bar{p}p}$ is the reduced mass of $\bar{p}p$. For $(N,L) = (41,40)$, the collision energy $E = 5$ eV is below $|E_{NL}| = 16.347$ eV (Table II) and gives $n_{\max} = 34$, while $E = 50$ eV gives $n_{\max} = \infty$. It is observed that no $\bar{p}p$ formation takes place for n lower than a certain value $n_{\min}$. This means that the final kinetic energy ϵ of $\bar{p}p + \mathrm{He}^+$ has an upper limit. From Fig. 13, the lower limit $n_{\min}$ is only slightly dependent on E. For all the cases considered in this study, it can be empirically shown that $E_n > 3E_{NL}$ or $\epsilon < E + 2|E_{NL}|$.

The mean values of the final quantum numbers $\langle n\rangle$ and $\langle l\rangle$ are also plotted in Fig. 8. (It should be mentioned that the statistics might be insufficient if the exchange cross section is very small.) The mean value $\langle n\rangle$ is very close to the peak position of $\sigma(n)$ shown in Fig. 13 except for $(N,L) = (41,40)$ and $(61,60)$. The mean value $\langle l\rangle$ is mostly much lower than the peak position of $\sigma(l)$ shown in Fig. 13. In most cases, $\langle n\rangle$ and $\langle l\rangle$ are not so strongly dependent on E, and $\langle n\rangle$ is found to be roughly close to $n_{\rm c}$ given in Table II; namely, the mean value of the final n may be estimated from the condition of energy matching (i.e., $\epsilon \simeq E$). The CTMC study of $\bar{p} + \mathrm{H}_2^+$ collisions [5] shows however that the mean final quantum number $\langle n\rangle$ is much lower than the one expected from the energy matching condition: This is because the Coulomb attraction works even at very large distances between $\bar{p}$ and H_2^+. In $p + \bar{p}\mathrm{He}^+$, the difference $\langle n\rangle - \langle l\rangle$ is not large for the circular states with $N \lesssim 40$; e.g., $\langle n\rangle - \langle l\rangle = 4 \sim 6$ for $(N,L) = (32,31)$, and $\langle n\rangle - \langle l\rangle = 7 \sim 10$ for $(N,L) = (41,40)$ at all the energies. For the circular states with $N \gtrsim 50$, however the difference $\langle n\rangle - \langle l\rangle$ becomes significant especially at high energies where $\sigma_{\rm dis} > \sigma_{\rm ex}$.

VIII. SUMMARY

The PES based on the BO approximation for three-body $p + \bar{p}\mathrm{He}^+$ collisions was calculated in an *ab initio* manner. Using this PES, the CTMC calculations were carried out for the $\bar{p}$ exchange and dissociation reactions. The reaction cross sections and the product-state distributions in the exchange reaction were investigated for 15 highly excited initial orbital states of $\bar{p}\mathrm{He}^+$. The dependencies of the reactivity on the collision energy and on the initial state were discussed.

The orbital energy or the size of $\bar{p}\mathrm{He}^+$ is an important parameter characterizing both the exchange and dissociation reactions. The total reactivity is always promoted by high orbital motion. In the exchange reaction, the mean principal quantum number of the products $\bar{p}p$ is roughly estimated from the energy matching condition. The $\bar{p}p$ atoms in near-circular

states can be efficiently produced from the circular states of $\bar{p}He^+$. The exchange cross section vanishes at low collision energies in the case that the $\bar{p}He^+$ atoms are in circular or near-circular states. One can expect that the $\bar{p}He^+$ atoms in circular states are exceptionally stable against not only Auger but also collisional processes. The selectivity behavior of the exchange reaction for the orbital type of the initial target state is absent in the $p + \bar{p}p$ system owing to the hydrogenic degeneracy of the target.

The collision processes in $p + \bar{p}He^+$ can be investigated in the same way as the chemical reaction approach. However, since the $\bar{p}He^+$ atom is a complete dipole and also a high-speed rotor, the reaction dynamics can stand sharp distinction from that in the ordinary molecular system. As well as the studies on $\bar{p} + H_2^+$ [4,5,7,9] and on $H_2 + \bar{p}He^+$ [20–24,26], the present study, founded upon the concept of chemical reaction, provides an interesting view of atomic and molecular collision processes involving antiprotons.

[1] E. Fermi and E. Teller, Phys. Rev. **72**, 399 (1947).
[2] A. S. Wightman, Phys. Rev. **77**, 521 (1950).
[3] K. Sakimoto, Phys. Rev. A **82**, 012501 (2010).
[4] K. Sakimoto, Phys. Rev. A **69**, 042710 (2004).
[5] K. Sakimoto, J. Phys. B **37**, 2255 (2004).
[6] *Atomic-Molecule Collision Theory*, edited by R. B. Bernstein (Plenum, New York, 1979).
[7] J. S. Cohen, J. Phys. B **38**, 441 (2005).
[8] K. Sakimoto, Chem. Phys. Lett. **393**, 245 (2004).
[9] N. Zurlo *et al.*, Phys. Rev. Lett. **97**, 153401 (2006).
[10] T. Yamazaki, N. Morita, R. Hayano, E. Widmann, and J. Eades, Phys. Rep. **366**, 183 (2002).
[11] M. Hori, Phys. Rep. **403–404**, 337 (2004).
[12] R. S. Hayano, M. Hori, D. Horváth, and E. Widmann, Rep. Prog. Phys. **70**, 1995 (2007).
[13] G. T. Condo, Phys. Lett. **9**, 65 (1964).
[14] V. I. Korobov and I. Shimamura, Phys. Rev. A **56**, 4587 (1997).
[15] J. E. Russell, Phys. Rev. Lett. **23**, 63 (1969).
[16] R. Ahlrichs, O. Dumbrajs, H. Pilkuhn, and H. G. Schlaile, Z. Phys. A **306**, 297 (1982).
[17] I. Shimamura, Phys. Rev. A **46**, 3776 (1992).
[18] O. I. Tolstikhin, S. Watanabe, and M. Matsuzawa, Phys. Rev. A **54**, R3705 (1996).
[19] K. Sakimoto, Phys. Rev. A **84**, 032501 (2011).
[20] T. Yamazaki *et al.*, Chem. Phys. Lett. **265**, 137 (1997).
[21] B. Ketzer *et al.*, J. Chem. Phys. **109**, 424 (1998).
[22] B. Ketzer *et al.*, Eur. Phys. J. D **13**, 305 (2001).
[23] B. Juhász *et al.*, Chem. Phys. Lett. **379**, 91 (2003).
[24] B. Juhász *et al.*, Chem. Phys. Lett. **427**, 246 (2006).
[25] S. Sauge and P. Valiron, Chem. Phys. **265**, 47 (2001).
[26] S. Sauge and P. Valiron, Chem. Phys. **283**, 433 (2002).
[27] B. D. Obreshkov, D. D. Bakalov, B. Lepetit, and K. Szalewicz, Phys. Rev. A **69**, 042701 (2004).
[28] T. G. Winter, M. D. Duncant, and N. F. Lane, J. Phys. B **10**, 285 (1977).
[29] H. Goldstein, *Classical Mechanics* (Addison-Wesley, London, 1950).
[30] S. Bradenbrink, H. Reihl, T. Wörmann, Z. Roller-Lutz, and H. O. Lutz, J. Phys. B **27**, L391 (1994).
[31] D. S. Fisher, S. R. Lundeen, C. W. Fehrenbach, and B. D. DePaola, Phys. Rev. A **63**, 052712 (2001).
[32] A. N. Perumal and D. N. Tripathi, Phys. Rev. A **64**, 042709 (2001).
[33] T. B. Day, G. A. Snow, and J. Sucher, Phys. Rev. Lett. **3**, 61 (1959).
[34] M. Leon and H. A. Bethe, Phys. Rev. **127**, 636 (1962).
[35] K. Sakimoto, J. Phys. B **38**, 3447 (2005).